Int. J. Heat Mass Transfer. Vol. 30, No. 2, pp. 319–331, 1987
Printed in Great Britain

0017-9310/87 $3.00 + 0.00
Pergamon Journals Ltd.

Free convection heat transfer in a partially divided vertical enclosure with conducting end walls

E. ZIMMERMAN* and S. ACHARYA
Mechanical Engineering Department, Louisiana State University, Baton Rouge, LA 70803, U.S.A.

(*Received* 24 *October* 1985 *and in final form* 11 *June* 1986)

Abstract—A numerical study has been made of natural convection in an enclosure with perfectly conducting horizontal end walls and finitely conducting baffles. Results obtained using the Boussinesq model for density variation show good agreement with reported measurements of natural convection in a partitioned enclosure. Except at low Rayleigh numbers, a separation bubble is observed behind the baffle. The strength of the separation bubble increases while the strength of the main flow (moving up the hot wall and down the cold one) decreases with increasing baffle conductivity. The average Nusselt number for the enclosure is significantly smaller in the presence of the baffles. Except at low Rayleigh numbers (where baffle conductivity has little influence) the Nusselt number values decrease with increasing baffle conductivity.

INTRODUCTION

NATURAL convection in enclosures is of significant interest in the areas of solar collector design, electronic cooling, design of energy efficient buildings, etc. In view of this, the subject has received a fair amount of attention in the literature. Ostrach [1] and Catton [2] have reviewed the heat transfer literature pertaining to enclosure convection.

More recently, heat transfer in partially divided enclosures has received limited attention primarily due to its application in the design of energy efficient buildings. Probert and Ward [3] experimentally studied the heat transfer behavior in a partitioned enclosure with aspect ratios of 18.2 and 26.4. Janikowski *et al.* [4] extended the work in ref. [3] to investigate the thermal resistance of an air filled enclosure with an aspect ratio of 5 and fitted with vertical baffles extending from the floor and ceiling. Greif and co-workers have conducted a series of experiments [5–7] to study the heat transfer behavior in an enclosure of aspect ratio 0.5 and fitted with a downward-extending partition. Experiments were generally carried out with water as the working fluid and for Rayleigh numbers in the range of 10^{10}–10^{11}. Duxbury [8] studied the heat transfer behavior in enclosures of aspect ratios between 5/8 and 5 with different partition arrangements. His results indicate significant heat losses from the side walls. Winters [9] performed a finite-difference study of natural convection in a vertical enclosure with an aspect ratio of 5/8 and fitted with centrally located baffles. Although the results in refs. [8, 9] agree qualitatively, significant quantitative differences were noted and were attributed to the side wall heat losses in the experimental setup in ref. [8] and the assumption of adiabatic side walls in ref. [9]. Lin and Bejan [10] carried out an experimental and analytical investigation for a rectangular enclosure (aspect ratio = 0.3) fitted with a single baffle.

Recently, Chang and co-workers [11, 12] have reported detailed numerical computations of natural convection in a square enclosure fitted with adiabatic partitions extending from the floor and ceiling (Fig. 1). Results were obtained for Rayleigh numbers in the range of 10^4–10^8 and radiation effects were also considered. As a follow-up of the work in refs. [11, 12], Bajorek and Lloyd [13] made an experimental study of heat transfer in the same configuration (Fig. 1). A typical comparison of the results in refs. [11–13] is shown in Fig. 2. It is clear that the experimentally determined Nusselt numbers are significantly higher than the predicted values. To explain this discrepancy, it should be noted that in the numerical calculations [11, 12], the end walls and partitions were assumed to be adiabatic. In the experiments, Bajorek and Lloyd [13] used Plexiglass side walls and baffles which have a thermal conductivity nearly 25 times that of air. Thus, as pointed out by El-Sherbiny *et al.* [14], adiabatic conditions are unlikely to be realized.

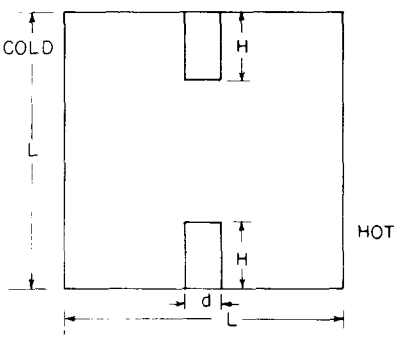

FIG. 1. Schematic of a square enclosure fitted with two baffles.

* Present address: Department of Mechanics, United States Military Academy, West Point, NY 10996-1792, U.S.A.

NOMENCLATURE

c_p	specific heat of fluid
d	thickness of the baffle
g	gravitational force
H	height of the baffle
k	thermal conductivity of fluid
k_r	conductivity ratio, k_s/k
k_s	conductivity of baffle
L	dimensions of the square enclosure
Nu	Nusselt number, hL/k
Nu_h	Nusselt number along hot wall
$\overline{Nu}$	average Nusselt number
$\overline{Nu}_h$	average Nusselt number along hot wall
p	thermodynamic pressure
P	dimensionless pressure
Pr	Prandtl number, $\mu c_p/k$
Ra	Rayleigh number, $g\beta(T_h - T_c)L^3/\nu\alpha$
Ra_y	local Rayleigh number, $g\beta\Delta T y^3/\nu\alpha = Ra(y/L)^3\,\Delta T/(T_h - T_c)$
T	dimensional temperature
T_c	cold wall temperature
T_h	hot wall temperature
u	dimensional velocity in the x direction
U	dimensionless velocity in the x direction
v	dimensional velocity in the y direction
V	dimensionless velocity in the y direction
x, X	dimensional and dimensionless coordinate parallel to the horizontal end walls
y, Y	dimensional and dimensionless coordinate normal to the horizontal end walls.

Greek symbols

β	thermal diffusivity
ν	kinematic viscosity
ρ	density
θ	dimensionless temperature
θ_s	dimensionless temperature in baffle
ψ	dimensionless stream function.

However, for a two-partition square enclosure, the work in refs. [11, 12] represents the only source for detailed velocity and temperature information.

The work reported in this paper was initiated with the intent of reporting numerical calculations that would compare favorably with the measurements in ref. [13] which report only mid-height temperature profiles and local and average Nusselt numbers and to provide detailed temperature, velocity and heat transfer information over a range of Rayleigh numbers. Since adiabatic conditions are unlikely to be realistic [14], the end walls are assumed to be perfectly conducting while the baffles are considered to have finite thermal conductivity. The assumption of perfectly conducting end walls is based primarily on an earlier study by the authors [15] where the predictions in a vertical enclosure with either adiabatic or perfectly conducting end walls are compared with the measurements reported by Krane and Jesse [16] where the end walls were made of balsa wood backed with insulation and have a thermal conductivity 27% higher than that of air. This comparison is reproduced in Fig. 3 which plots the predicted and measured velocity profiles and Nusselt number distributions and clearly confirms the superiority of the perfectly conducting end wall assumption. For Plexiglass end walls, the perfectly conducting end wall assumption is likely to yield more realistic results in view of the higher thermal conductivity of Plexiglass compared to insulation backed balsa wood.

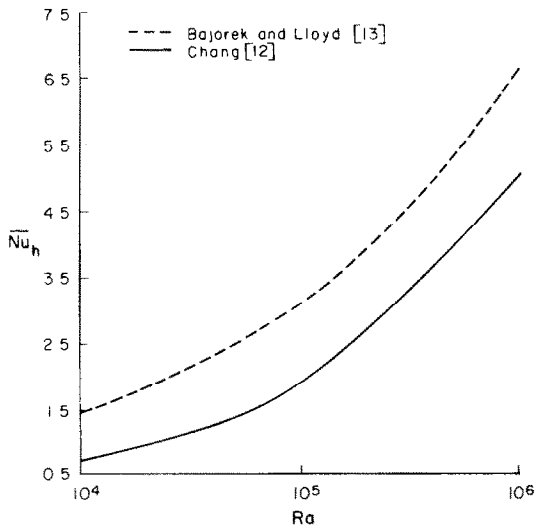

FIG. 2. Average Nusselt number comparison between the predictions in ref. [12] and measurements in ref. [13].

It should be clearly pointed out that the present study differs from that reported in refs. [11, 12], in which the end walls and baffles are assumed to be adiabatic. In this paper, as discussed above, in order to obtain realistic predictions, the end walls are assumed to be perfectly conducting and the baffles are assumed to have a finite thermal conductivity (which is varied as a parameter of interest) and no numerical solutions have, heretofore been reported in the literature, with these assumptions. As discussed later in the paper, results obtained with the aforementioned assumptions, agree reasonably well with measurements, while corresponding calculations done with assumed adiabatic end walls but finitely conducting baffles [23] exhibit much larger discrepancies. These discrepancies are expected to be even larger if the baffles are also assumed to be adiabatic as in refs. [11, 12].

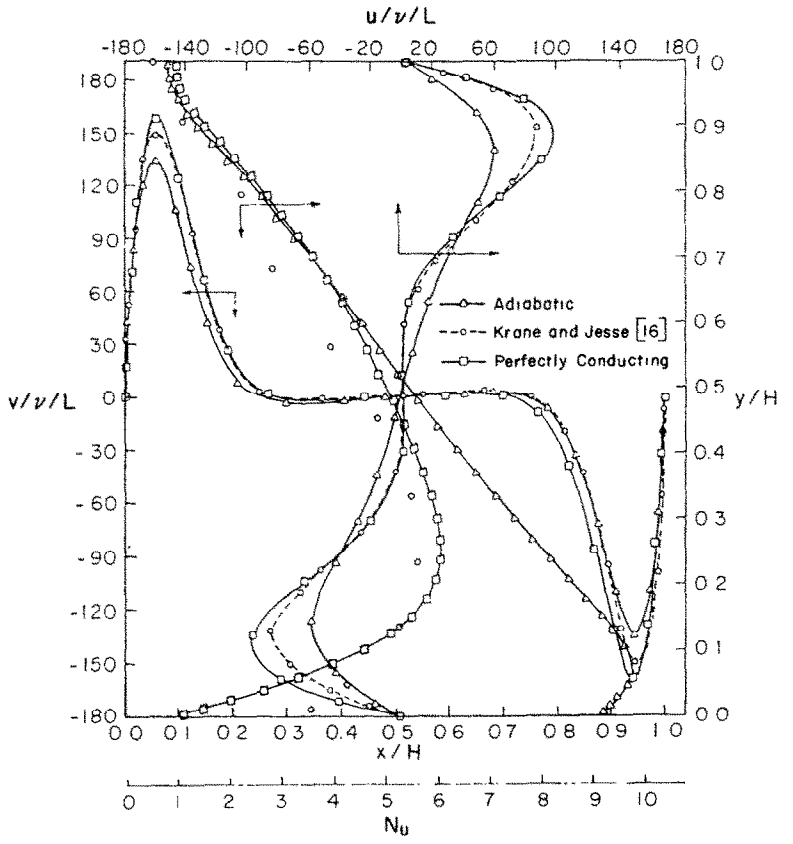

FIG. 3. Comparison of predicted and measured velocity and Nusselt number profiles at $Ra = 1.89 \times 10^5$: implications of the choice of end wall conditions.

GOVERNING EQUATIONS

The schematic of the physical situation of interest is shown in Fig. 1. The dimensions of the baffle and box are chosen to correspond with the physical dimensions employed by Bajorek and Lloyd [13]. Typical temperature differences in ref. [13], between the hot wall (at T_h) and cold wall (maintained at room temperature T_c) are of the order of 15.5°C at a Rayleigh number of 3.5×10^5. With these temperature differences, the temperature ratio $(T_h - T_c)/T_c \cong 0.05$ and therefore, the Boussinesq approximation, which has been shown by Zhong [17] to be valid for $(T_h - T_c)/T_c \leqq 0.1$, should correctly model the density variation. The adequacy of the Boussinesq approximation is further examined here by comparison with the predictions obtained using the ideal gas law to calculate the density.

In addition to the Boussinesq approximation, the flow is assumed to be steady, laminar and two-dimensional. These assumptions, for the Rayleigh numbers of interest in this study, have been verified experimentally in a number of studies [18–20]. Radiation effects, which are small for moderate temperature differences, have not been included. With these assumptions and the introduction of the following dimensionless variables

$$X = x/L, \qquad Y = y/L \tag{1}$$

$$U = u/(\nu/L), \qquad V = v/(\nu/L),$$

$$P = (p + \rho g y)/[\rho(\nu/L)^2] \tag{2}$$

$$\theta = [T - (T_h + T_c)/2]/(T_h - T_c) \tag{3}$$

the governing differential equations that express the conservation of mass, momentum and energy in the fluid become

$$\partial U/\partial X + \partial V/\partial Y = 0 \tag{4}$$

$$U\partial U/\partial X + V\partial U/\partial Y = -\partial P/\partial X + \partial^2 U/\partial X^2 + \partial^2 U/\partial Y^2 \tag{5}$$

$$U\partial V/\partial X + V\partial V/\partial Y = -\partial P/\partial Y + \partial^2 V/\partial X^2 + \partial^2 V/\partial Y^2 + Ra \cdot \theta/Pr \tag{6}$$

$$U\partial\theta/\partial X + V\partial\theta/\partial Y = (\partial^2\theta/\partial X^2 + \partial^2\theta/\partial Y^2)/Pr. \tag{7}$$

In the baffle region, the velocities are zero and the temperature in the baffle θ_s is described by Laplace's equation

$$(\partial^2\theta_s/\partial X^2 + \partial^2\theta_s/\partial Y^2) = 0. \quad (8)$$

The energy balance at the baffle–air interface requires

$$\left(-k\frac{\partial T}{\partial n}\right)_{\text{interface}} = \left(-k_s\frac{\partial T_s}{\partial n}\right)_{\text{interface}}$$

or

$$(1/Pr)(-\partial\theta/\partial n)_{\text{interface}} = [(k_s/k)/Pr](-\partial\theta_s/\partial n)_{\text{interface}} \quad (9)$$

where k_s represents the thermal conductivity of the baffle and $[(k_s/k)/Pr]$ is the dimensionless baffle conductivity. For convenience in notation, the conductivity ratio k_s/k is denoted by k_r.

The boundary conditions are zero velocity on all four walls, dimensionless temperatures of 0.5 and -0.5 along the hot and cold vertical walls, respectively, and perfectly conducting (linear temperature profile) horizontal end walls.

SOLUTION PROCEDURE

Equations (4)–(9) provide a complete mathematical specification to the problem and are solved by a control volume based, finite-difference calculation procedure called SIMPLER (Semi Implicit Method for Pressure Linked Equations Revised) which has been described in detail by Patankar [21]. In this method, the domain is discretised into a number of control volumes (each associated with a nodal point) such that a control volume face coincides with the baffle–air interface. The finite-difference equations are obtained by requiring that the conservation of mass, momentum and energy be satisfied over each control volume. To promote the conservative property, it is required that the flux leaving a control volume through a face must equal the flux entering the adjoining control volume through the same face. To avoid checkerboard pressure and velocity fields, a staggered grid for velocity is used. The pressure–velocity interlinkage is handled by a prediction–correction approach in which the velocity is first estimated by solving the momentum equations and then updated by requiring that continuity be satisfied in each control volume. The finite-difference equations are solved iteratively by a line-by-line Thomas Algorithm.

The presence of the baffle in the solution domain is accounted for by the strategy suggested by Patankar [22], in which equations (4)–(7) are solved in the entire domain and the baffle is characterized as a region of very high viscosity (say 10^{30}) and the dimensionless baffle conductivity k_r/Pr. In view of the very high viscosity and no-slip boundary conditions, the velocities in the baffle region are nearly zero and therefore, the convective terms in equation (7) drop out and the energy equation reduces to Laplace's equation [equation (8)] in the baffle. The interface energy balance [equation (9)] is also satisfied since the baffle–air interface coincides with a control volume face and the dimensionless heat flux leaving the fluid control volume through the interface must equal the interface heat flux entering the baffle control volume, i.e.

$$(1/Pr)(-\partial\theta/\partial n)_{\text{interface}} = (k_r/Pr)(-\partial\theta_s/\partial n)_{\text{interface}}.$$

A 40 × 40 non-uniform grid is used in the calculation with the grid point distribution carefully tailored to yield numerically accurate results. The numerical accuracy of the results is verified by comparing the 40 × 40 grid solutions with the corresponding solutions obtained on an 80 × 80 grid. This comparison is shown in Fig. 4 and confirms the adequacy of the 40 × 40 grid. Overall conservation of momentum and energy are satisfied to within 1% with the 40 × 40 mesh.

RESULTS AND DISCUSSIONS

Results are presented in two parts. In the first part, the predicted mid-height temperature profiles and hot and cold wall Nusselt numbers are compared with the measurements reported in ref. [13]. As will be seen later, the agreement between measurements and predictions is good thus validating the assumptions made in this paper. The second part complements the rather limited measurements in ref. [13] and provides detailed velocity, temperature and heat transfer information for an enclosure with finitely conducting baffles and perfectly conducting end walls. The Rayleigh number Ra, baffle thickness (d/L) and conductivity ratio k_r are the primary parameters of interest in this study.

Comparison with measurements [13]

In ref. [13], the baffles were made of Plexiglass and the dimensionless thickness (d/L) and height (H/L) were 0.1 and 0.25, respectively. In this paper, results are obtained for the same geometrical dimensions and in the first part of this study, the conductivity ratio k_r is assigned a value representative of Plexiglass material. Also, to test the validity of the Boussinesq approximation, results are obtained using both the Boussinesq model and the variable density model $(\rho = p/RT)$. Details regarding the dimensionless variables and governing equations in the variable density model are presented in refs. [15, 23].

Figure 5 presents the predicted mid-height temperature profile and the mid-sectional velocity profiles and also, the temperature distribution measured in ref. [13]. Predictions include both the Boussinesq and the variable density model solutions for both the velocity and temperature and confirm the adequacy of the Boussinesq approximation at the Rayleigh number considered ($Ra = 3.5 \times 10^5$). The measured

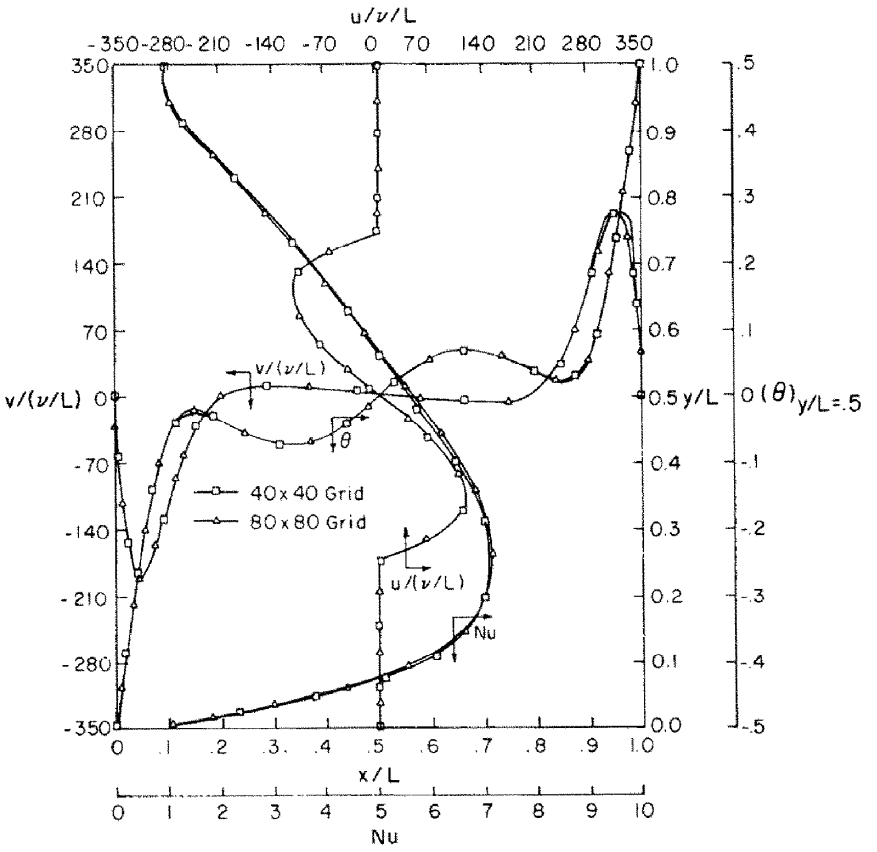

FIG. 4. Effect of mesh refinement on predictions.

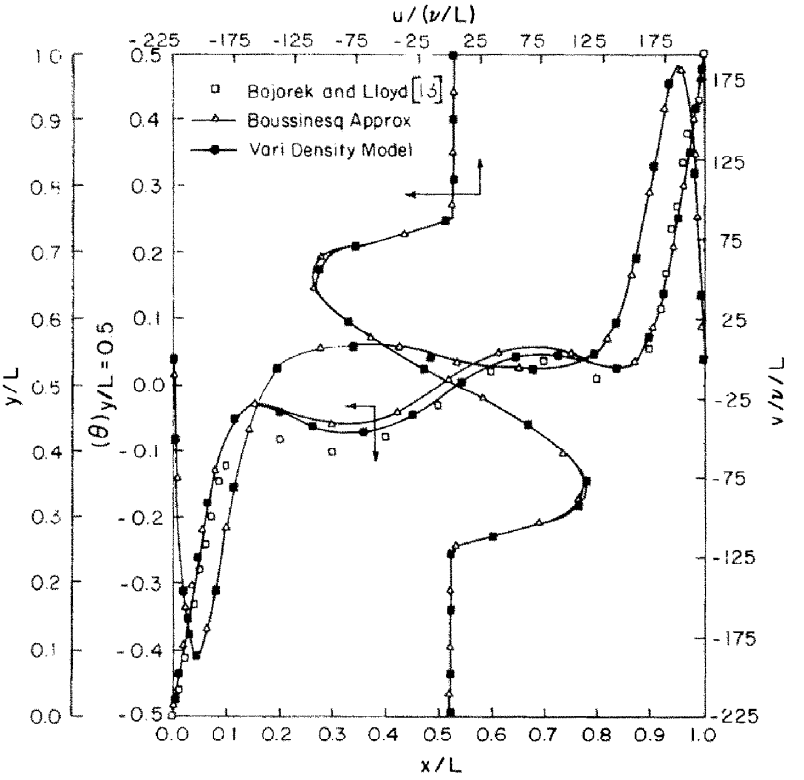

FIG. 5. Comparison of temperature profile with measurements in ref. [13] and mid-sectional velocity profiles.

and predicted temperature profiles in Fig. 5 agree well with each other with a 4.4% maximum discrepancy between the two profiles. As further verification, Zimmerman [23] made extensive calculations for natural convection in a non-partitioned enclosure using the experimentally measured end wall temperatures by Krane and Jesse [16] as end wall boundary conditions (to eliminate the uncertainty associated with the end wall boundary condition). The comparison of the Boussinesq and the ideal gas law predictions [23] for the velocity and temperature with the measurements [16] show excellent agreement with each other. The velocity profiles in Fig. 5 exhibit the expected behavior with a boundary layer profile near the hot and cold walls and a lower peak horizontal velocity compared to the peak vertical velocity.

Figure 6 compares the predicted and measured hot wall Nusselt number distribution. In general, the agreement is good. The predicted value for the average hot wall Nusselt number at $Ra = 3.5 \times 10^5$ is 4.3 while the corresponding measured value is 4.65. The present predictions exhibit much closer agreement with the measured values than the predictions in ref. [11] where the baffles and end walls were assumed to be adiabatic.

Additional results for an enclosure with conducting end walls

In this section, results are presented for Rayleigh numbers in the range of 10^4–3.55×10^5, conductivity ratios of 2 and 500 and dimensionless baffle thicknesses of 0.05, 0.1 and 0.2. Results presented include streamline and isotherm plots, mid-sectional velocity and temperature information and local and average Nusselt numbers.

Streamline and isotherm plots. Streamlines and isotherms are shown in Figs. 7–10 with the streamlines plotted in uniform increments of $\Delta\psi$ (from a lower bound of ψ_l to an upper bound of ψ_u) and the isotherms plotted in uniform increments of 0.05 (from -0.5 at the cold wall to 0.5 at the hot wall). The values of ψ_l, ψ_u and $\Delta\psi$ are indicated on the top right corner of the figure as $(\psi_l, \psi_u)\Delta\psi$. The maximum streamfunction value ψ_m is also shown on the figure.

At a Rayleigh number of 10^4, the isotherm plot (not shown) is nearly conduction like and the natural convection flow is rather weak ($\psi_m \cong 3.3$). For both conductivity ratios, the flow at $Ra = 10^4$, does not separate behind the baffle. As the Rayleigh number is increased to 10^5, the flow for the higher baffle conductivity ($k_r = 500$) separates behind the baffle (Fig. 7b) although, at $k_r = 2$, a noticeable separation bubble is not predicted. To explain this, it should be noted that for $k_r = 500$, the baffle temperatures are expectedly closer (compared to the corresponding temperatures for $k_r = 2$) to the dimensionless end wall temperature of zero (at $x/L = 0.5$) and therefore, at the higher baffle conductivity, the upper baffle is colder and the lower baffle is warmer relative to the baffle temperatures at $k_r = 2$. The cooled fluid off the cold wall is heated to a higher temperature as it

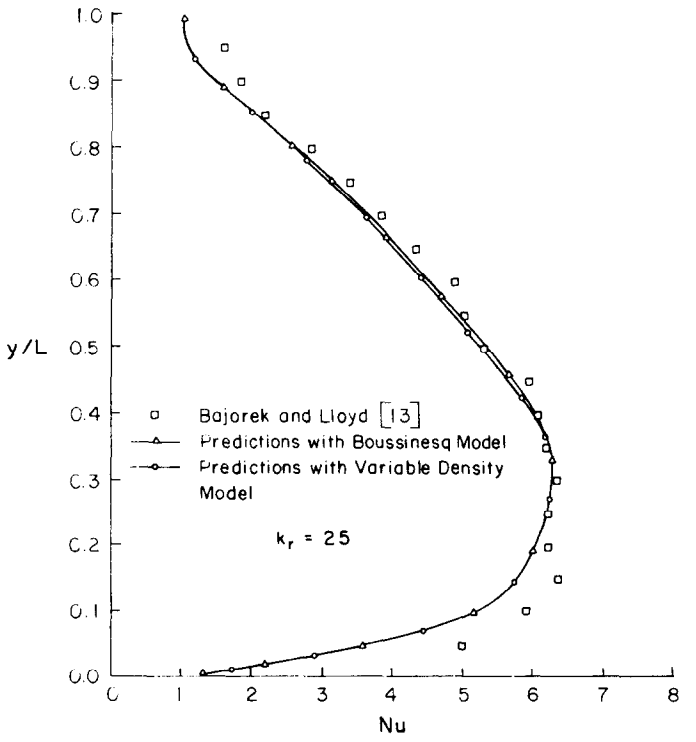

FIG. 6. Comparison of predicted and measured [13] Nusselt numbers.

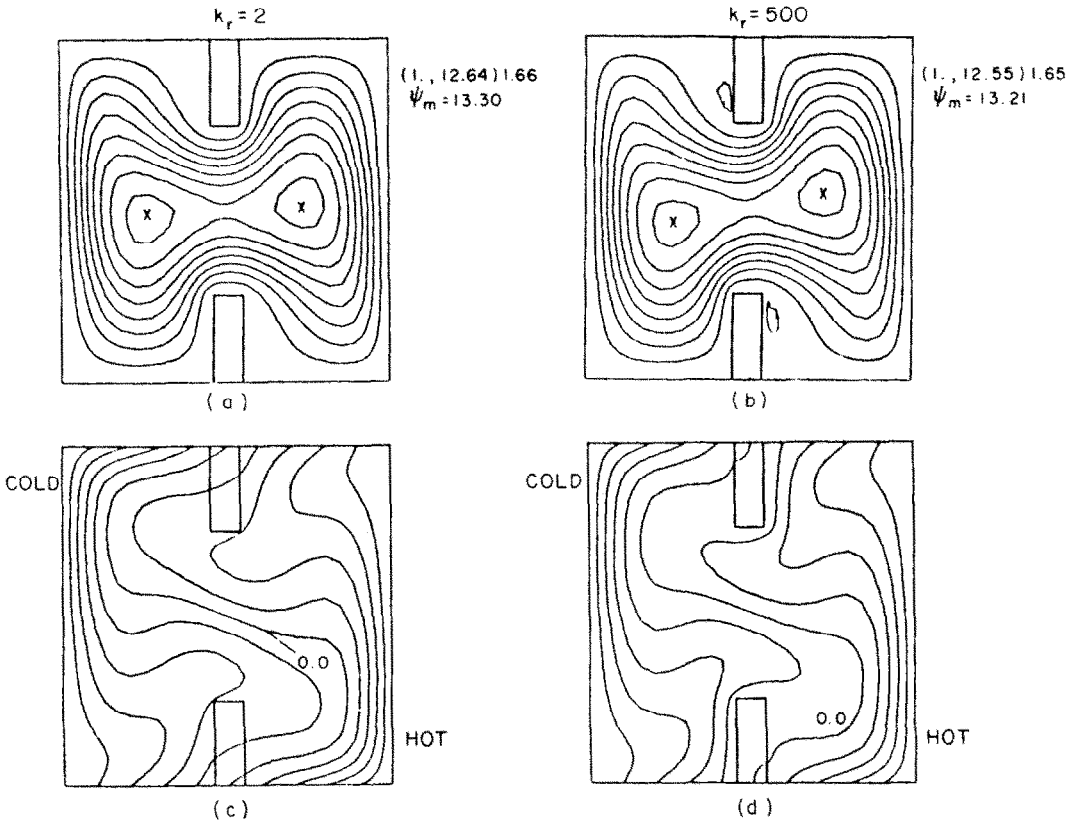

FIG. 7. Streamlines and isotherms at $Ra = 10^5$, $d/L = 0.1$.

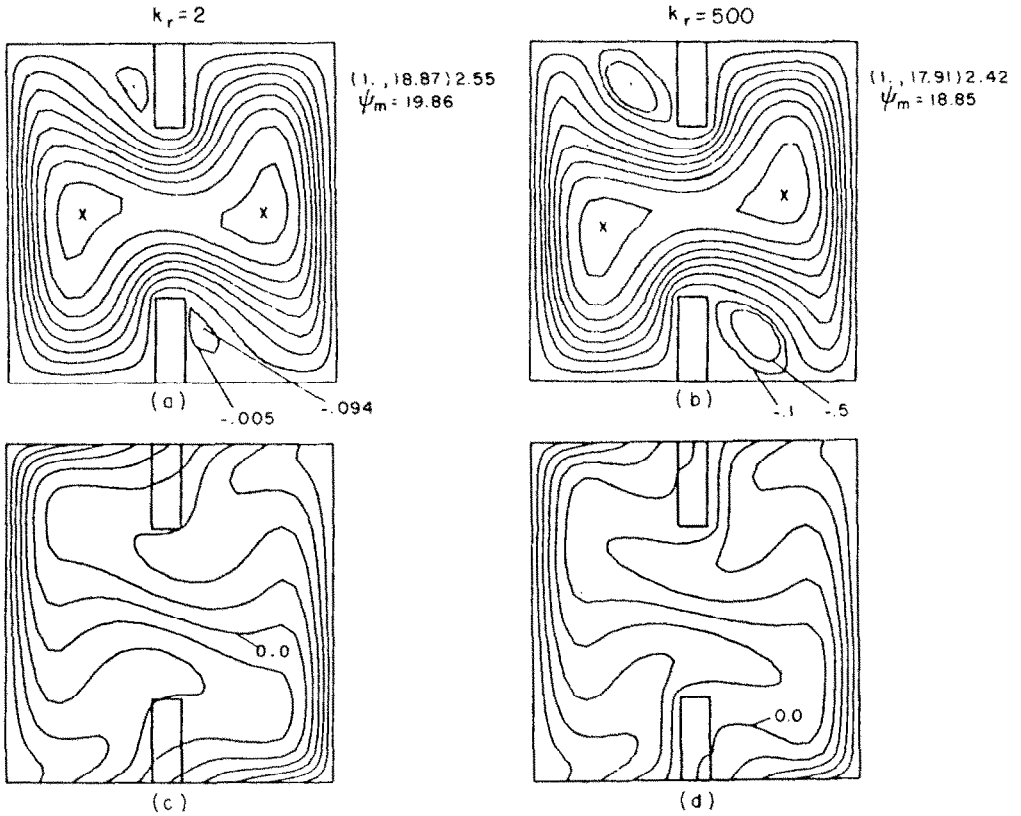

FIG. 8. Streamlines and isotherms at $Ra = 3.55 \times 10^5$, $d/L = 0.1$.

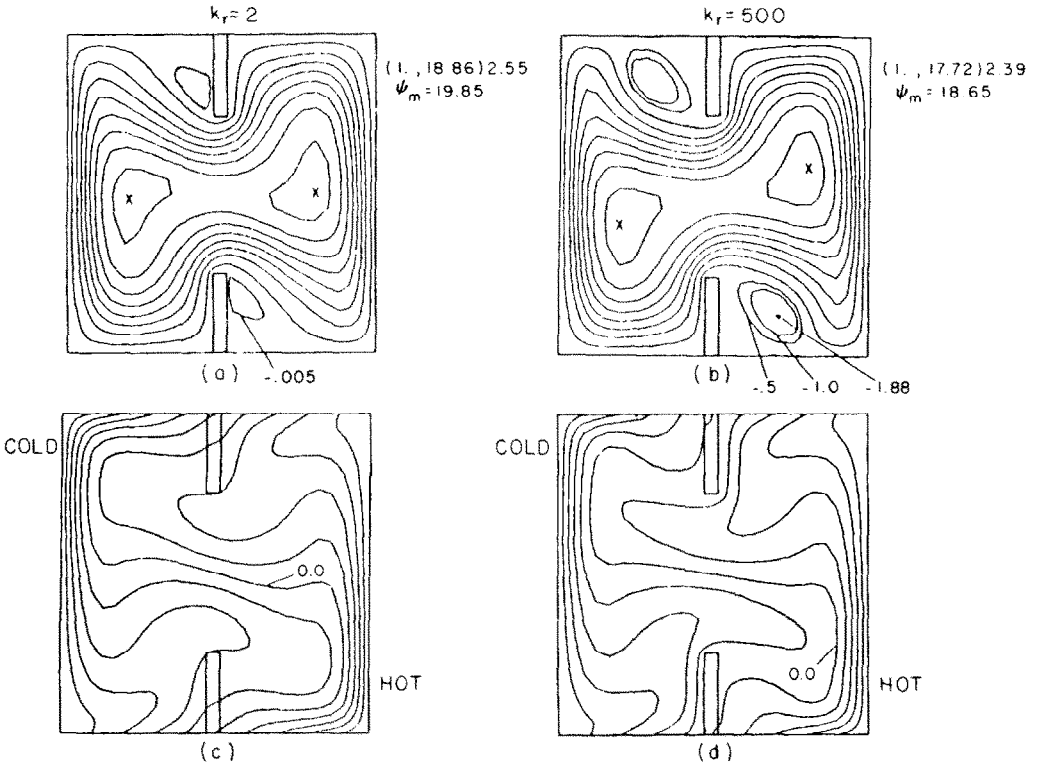

FIG. 9. Streamlines and isotherms at $Ra = 3.55 \times 10^5$, $d/L = 0.05$.

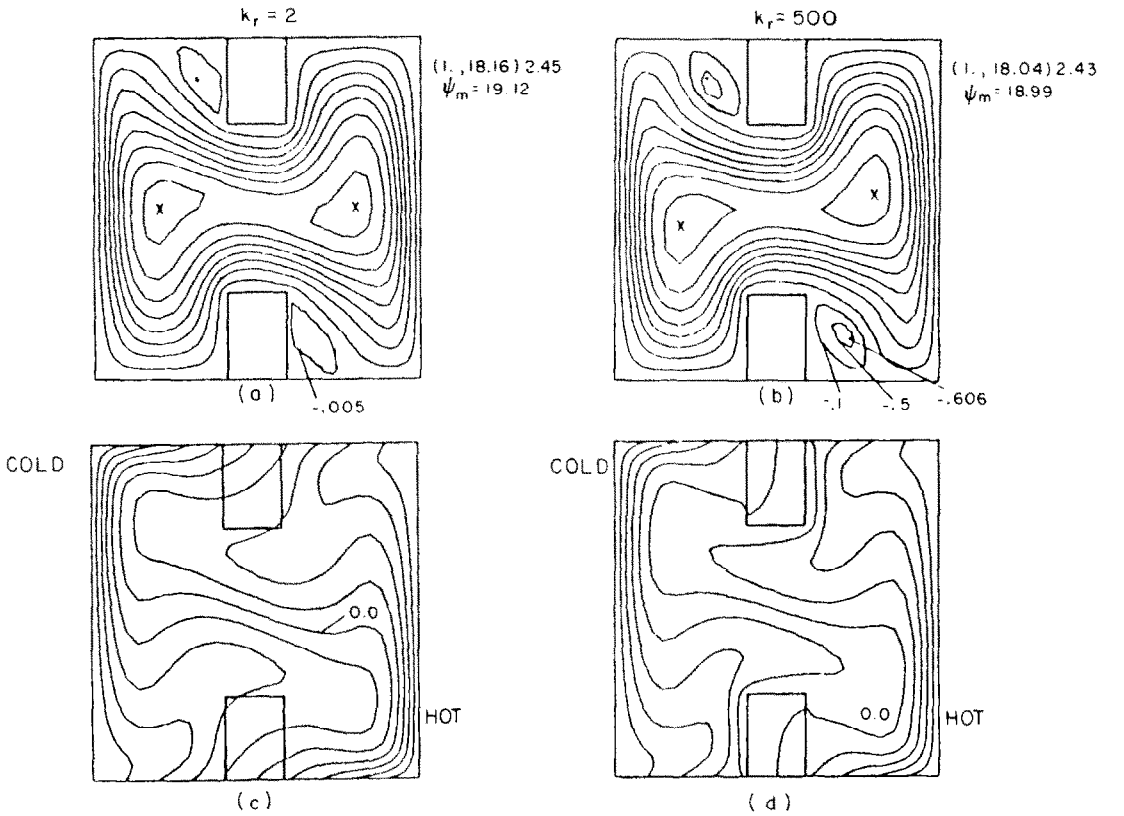

FIG. 10. Streamlines and isotherms at $Ra = 3.55 \times 10^5$, $d/L = 0.2$.

negotiates the higher conductivity lower baffle (since it is warmer) and therefore, at $k_r = 500$, the warmer flow at the lower baffle tip is more buoyant than the corresponding flow at $k_r = 2$. Since the tendency of the flow to move downwards is less for the more buoyant flow, flow separation is more easily effected at the higher k_r value. For this reason, a large recirculation is noted behind the higher conductivity baffle. A similar explanation applies to the separation bubble behind the upper baffle.

As the Rayleigh number is increased to 3.55×10^5 (Fig. 8), the strength of the flow field increases and the separation bubbles grow in size, with separation now occurring even behind the lower conductivity baffle. As k_r is increased from 2 (Fig. 8a) to 500 (Fig. 8b), the size and strength of the recirculation bubble increases since, as mentioned in the preceding paragraph, the flow at the tip of the upward-extending baffle is warmer and that at the tip of the downward-extending baffle is colder for the higher baffle conductivity. However, the velocities in the main eddy (with flow up the hot wall and down the cold one) are reduced as k_r is increased. This is because the increased cooling by the upper baffle and the increased heating by the lower baffle at the higher baffle conductivity reduces the local wall to fluid temperature difference ΔT and thus the local Rayleigh number $[Ra_y = Ra(y/L)^3 \Delta T/(T_h - T_c]$ at the leading edge of the hot and cold walls. In view of the lower local Rayleigh numbers, the strength of the buoyancy induced flow along the hot and cold walls is reduced.

The influence of the baffle thickness (d/L) is shown in Figs. 9 $(d/L = 0.05)$ and 10 $(d/L = 0.2)$ and indicates that the qualitative behavior of the flow field and isotherm distributions are similar at both baffle thicknesses. However, significant quantitative differences can be noted. As (d/L) is increased from 0.05 to 0.2, the separation bubble behind the baffle ($k_r = 500$) decreases in strength while the velocities of the main flow (up the hot wall and down the cold wall) increase in magnitude. These effects are linked to the counteracting influences of increased viscous resistance and increased pre-cooling and pre-heating by the upper and lower baffles respectively at the higher (d/L) value.

The features of the flow pattern are in general agreement with the flow visualization experiments by Duxbury [8] and the numerical predictions of Winters [9] for an enclosure with a single baffle. Flow visualization studies have not been reported in the experimental studies on enclosures with two baffles [3–6, 13] and therefore, a direct comparison is not possible.

Temperature and velocity profiles. The mid-height temperature profiles for a baffle thickness $d/L = 0.1$ are shown in Fig. 11. At a Rayleigh number of 10^4, the temperature profile in view of the weak convective motion, is nearly linear and the baffle conductivity has a negligible effect on the temperature values. As the Rayleigh number is increased the temperature profile takes on a boundary layer behavior with large near-wall gradients and small temperature variations in the core. However, the core temperatures exhibit

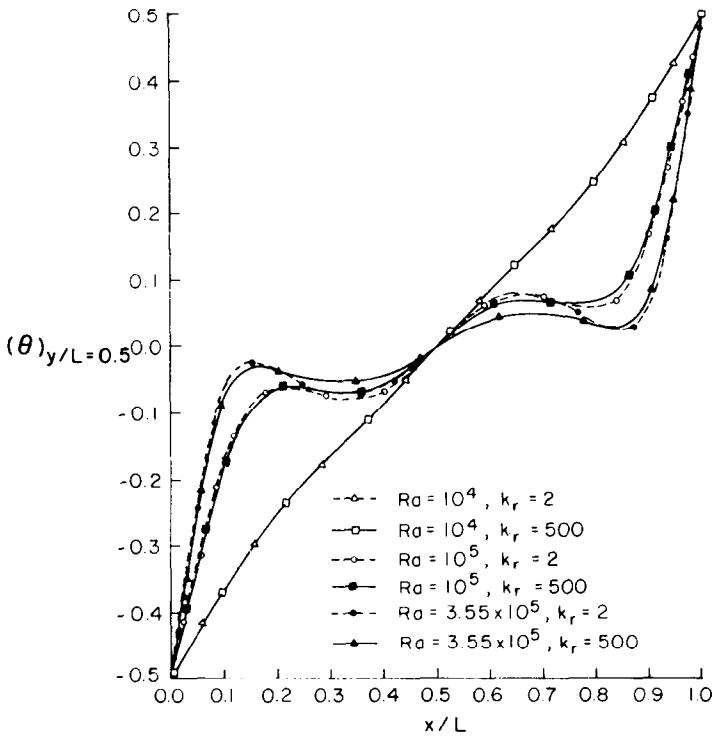

FIG. 11. Temperature profiles, $d/L = 0.1$, $y/L = 0.5$.

greater non-uniformity as compared to the core temperature profile in an enclosure without baffles. This is due to the mixing of the fluid heated by the lower baffle with the fluid cooled by the upper one, with the mixing in the cooler side of the enclosure influenced more by the colder fluid and that on the hot wall side influenced more by the warmer fluid. Thus, core temperatures near the cold wall are lower and those near the hot wall are higher than the corresponding temperatures in an enclosure without baffles. The non-uniformity of the core temperature is more pronounced at the lower conductivity value since the lower baffle is colder and the upper baffle is warmer at $k_r = 2$ compared to the temperatures at $k_r = 500$.

The vertical velocity profile at $y/L = 0.5$ and the horizontal velocity profile at $x/L = 0.5$ are shown in Fig. 12. Since the profiles are symmetrical, only half the profile is shown. Velocities expectedly increase with Rayleigh number and exhibit a boundary-layer behavior along the hot and cold walls at high Rayleigh numbers (3.55×10^5). In general, the mid-sectional velocity profiles exhibit a weak dependence on the conductivity ratio with the magnitude of the V-velocity in the boundary layer lower and that in the core higher at $k_r = 500$. The lower boundary-layer velocities at the higher baffle conductivity are, as mentioned earlier, attributable to the increased pre-cooling by the upper baffle and pre-heating by the lower baffle of the fluid directed towards the cold and hot walls respectively. Since mass flow rates across a cross-section must remain constant, increased boundary layer velocities are associated with depressed core velocities.

Table 1. Average Nusselt numbers

Ra	k_r	$d/L = 0.05$	$d/L = 0.1$	$d/L = 0.2$	No baffles
10^4	2	1.25	1.22	1.18	1.75
	500	1.25	1.22	1.20	
10^5	2	2.95	2.90	2.75	3.37
	500	2.74	2.69	2.52	
3.55×10^5	2	4.61	4.58	4.43	4.91
	500	4.18	4.14	4.01	

Nusselt number. The Nusselt number along the hot and cold walls is defined as

$$Nu = -L(\partial T/\partial x)_{\text{wall}}/(T_h - T_c). \tag{10}$$

The average Nusselt number $\overline{Nu}$ for the various cases studied is presented in Table 1. The average Nusselt number for an enclosure with no baffles and conducting end walls is also presented in the table for comparison purposes.

As may be expected, the heat transfer across the enclosure (or the average Nusselt number) is less in the presence of baffles and decreases with increasing baffle thickness. For $d/L = 0.1$, the heat transfer across the enclosure at $Ra = 10^4$ is reduced by approximately 30% due to the presence of the baffles and the average heat transfer is relatively unaffected by the conductivity ratio k_r. At the higher Rayleigh number of 3.55×10^5, the reduction in the average Nusselt number due to the baffles is approximately 16% for $k_r = 500$ (and $d/L = 0.1$) and about 7% for $k_r = 2$.

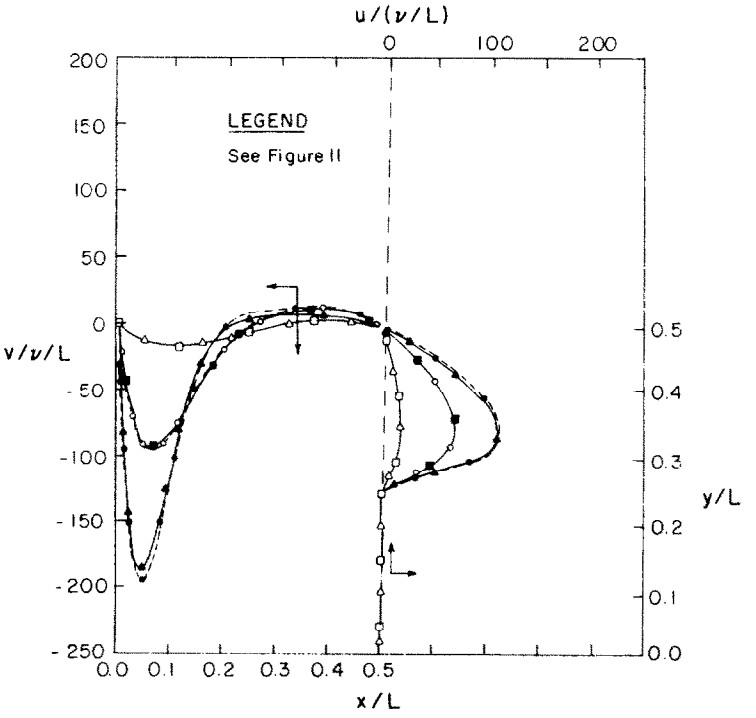

FIG. 12. Horizontal velocity (at $x/L = 0.5$) and vertical velocity (at $y/L = 0.5$) profiles, $d/L = 0.1$.

Thus, at the higher Rayleigh number, the conductivity ratio has a significant influence on the average heat transfer with an additional 7–10% reduction in the Nu value when the baffle conductivity ratio is higher ($k_r = 500$). This result, somewhat surprising at first glance, is due to the increased pre-heating and pre-cooling effects of the more conducting lower and upper baffles, respectively, which in turn is responsible for smaller wall to fluid temperature differences. It should be noted that the 16% reduction in Nu for the more conducting baffle at $Ra = 3.55 \times 10^5$ is in excellent agreement with the measured reduction of 17% in ref. [13] at $Ra = 3.5 \times 10^5$.

In order to further delineate the importance of using perfectly conducting end wall conditions, Table 2 has been compiled from the calculations in ref. [23] and the results reported in refs. [13, 16, 24]. Clearly, in all the cases listed, the predictions with the perfectly conducting end walls are closer to the measured values in refs. [13, 16] and the correlation for the perfectly conducting end wall in ref. [24]. Corresponding predictions with adiabatic end walls show significantly larger deviations from the measured values.

The local Nusselt number distribution along the hot wall is plotted in Fig. 13 and again shows lower local heat transfer rates for the enclosure with the

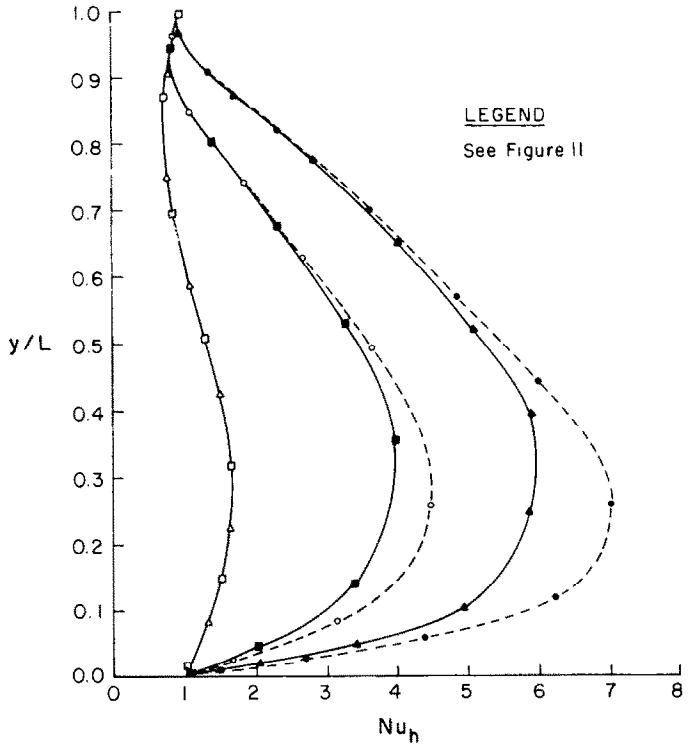

FIG. 13. Nusselt number distribution along hot wall, $d/L = 0.1$.

Table 2. Comparison of measured and predicted Nusselt numbers

Ra	Non-partitioned enclosures: Present predictions		Reported correlations or measurements			
	Perfectly conducting end walls	Adiabatic end walls	Ref. [13]*	Ref. [16]	Ref. [24] (Perfectly conducting end walls)†	Ref. [24] (Adiabatic end walls)‡
10^5	3.37	4.53	3.89	—	3.03	4.41
1.89×10^5	4.07	5.47	4.71	3.63	3.64	5.3
3.55×10^5	4.91	6.58	5.68	—	4.35	6.33

Ra	Partitioned enclosures: Present predictions			Reported correlations
	Perfectly conducting $k_r = 2$	Perfectly conducting $k_r = 25$‖	Adiabatic end walls $k_r = 2$	Ref. [13]§ $k_r = 25$‖
10^5	2.9	—	3.95	3.15
3.5×10^5	—	4.3	—	4.65
3.55×10^5	4.58	—	6.09	4.78

* $\overline{Nu} = 0.111(Ra/Pr)^{0.30}$.
† $\overline{Nu} = 0.114(Ra)^{0.285}$.
‡ $\overline{Nu} = 0.166(Ra)^{0.285}$.
§ $\overline{Nu} = 0.063(Ra/Pr)^{0.33}$.
‖ $k_r = 25$ corresponds to Plexiglass.

more conducting baffle. The plot shows the same trends as the Nusselt number distribution in an enclosure with no baffles except, and as expected, the peak Nusselt numbers in the presence of baffles occur at a higher (y/L) value.

CONCLUDING REMARKS

A numerical investigation is made of natural convection in a partitioned enclosure with conducting end walls. Results are compared with the measurements of Bajorek and Lloyd [13] and indicate that for moderate temperature differences, predictions obtained with the Boussinesq approximation and perfectly conducting end wall assumption, compare well with measurements while results with the adiabatic end wall condition, show significant deviation. At high Rayleigh numbers, the flow behind the baffle separates with the size and strength of the separated bubble increasing with the baffle conductivity. The strength of the main flow (moving up the hot wall and down the cold one) however decreases with increasing conductivity of the baffle. The core temperature profile exhibits greater non-uniformity as compared to the temperature variations in an enclosure without baffles. The average Nusselt number for an enclosure is significantly smaller in the pressure of baffles and decreases with increasing baffle conductivity.

REFERENCES

1. S. Ostrach, Natural convection in enclosures. In *Advances in Heat Transfer* (Edited by J. P. Hartnett and T. F. Irvine), Vol. 8. Academic Press, New York (1972).
2. I. Catton, Natural convection in enclosures, *Proc. Sixth Int. Heat Transfer Conference*, Vol. 6, pp. 13–31 (1962).
3. S. D. Probert and J. Ward, Improvements in the thermal resistance of vertical, air-filled, enclosed cavities, *Proc. Fifth Int. Heat Transfer Conference*, Tokyo, NC3.9, pp. 124–128 (1974).
4. H. E. Janikowski, J. Ward and S. D. Probert, Free convection in vertical, air filled rectangular cavities fitted with baffles, *Proc. 6th Int. Heat Transfer Conference*, Toronto (1978).
5. M. W. Nansteel and R. Greif, Natural convection in undivided and partially divided rectangular enclosures, *J. Heat Transfer* **103**, 623–629 (1981).
6. M. W. Nansteel and R. Greif, An investigation of natural convection in enclosures with two and three-dimensional partitions, *Int. J. Heat Mass Transfer* **27**, 561–571 (1984).
7. F. Bauman, A. Gadgil, R. Kammerud and R. Grief, Buoyancy driven convection in rectangular enclosures: experimental results and numerical calculations, Paper No. ASME-80-HT-66 (1980).
8. D. Duxbury, An interferometric study of natural convection in enclosed plane air layers with complete and partial central vertical division. Ph.D. thesis, University of Salford, U.K. (1979).
9. K. H. Winters, The effect of conducting divisions on the natural convection of air in a rectangular cavity with heated side walls, ASME Paper No. 82-HT-69.
10. N. N. Lin and A. Bejan, Natural convection in a partially divided enclosure, *Int. J. Heat Mass Transfer* **26**, 1867–1877 (1983).
11. L. C. Chang, J. R. Lloyd and K. T. Yang, A finite difference study of natural convection in complex enclosures, *Heat Transfer 1982, Proc. Seventh Int. Heat Transfer Conference*, Munich, Vol. 1, pp. 183–188 (1982).
12. L. C. Chang, Finite difference analysis of radiation–convection interactions in two-dimensional enclosures. Ph.D. thesis, Department of Aerospace and Mechanical Engineering, University of Notre Dame (May 1981).
13. S. M. Bajorek and J. R. Lloyd, Experimental investigation of natural convection in partitioned enclosures, *J. Heat Transfer* **104**, 527–532 (1982).
14. S. M. El-Sherbiny, K. G. T. Hollands and G. D. Raithby, Effect of thermal boundary conditions on natural convection in vertical and inclined air layers, *J. Heat Transfer* **104**, 515–520 (1982).
15. E. Zimmerman and S. Acharya, Natural convection in a vertical square enclosure with perfectly conducting end walls, *ASME Solar Energy Conference*, Anaheim, CA (1986).
16. R. J. Krane and J. Jesse, Some detailed field measurements for a natural convection flow in a vertical square enclosure, *ASME–JSME Thermal Engineering Joint Conference*, Vol. 1, pp. 323–329 (1983).
17. Z. Y. Zhong, Variable property natural convection and its interaction with thermal radiation. Ph.D. thesis, Department of Aerospace and Mechanical Engineering, University of Notre Dame (1983).
18. S. J. M. Linthorst, W. M. M. Schinkel and C. J. Hoogendoorn, Flow structure with natural convection in inclined air-filled enclosures. In *Natural Convection in Enclosures* (Edited by K. E. Torrance and I. Catton), ASME-HTD-Vol. 8, pp. 39–45. ASME, New York (1980).
19. J. N. Arnold, I. Catton and D. K. Edwards, Experimental investigation of natural convection in inclined rectangular regions of differing aspect ratios, *J. Heat Transfer* **98**, 67–72 (1976).
20. H. Ozoe, H. Sayama and S. W. Churchill, Natural convection in an inclined square channel, *Int. J. Heat Mass Transfer* **17**, 401–408 (1979).
21. S. V. Patankar, *Numerical Heat Transfer and Fluid Flow*. McGraw-Hill, New York (1980).
22. S. V. Patankar, A numerical method for conduction in composite materials, flow in irregular geometries and conjugate heat transfer, *Proc. 6th Int. Heat Transfer Conference*, Toronto, Vol. 3, p. 297 (1978).
23. E. B. Zimmerman, Natural convection in square partitioned enclosures. M.S. thesis, Louisiana State University (May 1985).
24. W. M. M. Schinkel, S. J. M. Linthorst and C. J. Hoogendoorn, The stratification of natural convection in vertical enclosures. In *Natural Convection in Enclosures* (Edited by K. E. Torrance and I. Catton), ASME-HTD-Vol. 8, pp. 31–38. ASME, New York (1980).

CONVECTION THERMIQUE NATURELLE DANS UNE ENCIENTE VERTICALE PARTIELLEMENT DIVISEE, AVEC DES PAROIS EN BOUT CONDUCTRICES

Résumé—On étudie numériquement la convection naturelle dans une enceinte avec des parois en bout parfaitement conductrices et des baffles normalement conductrices. Les résultats obtenus par le modèle de Boussinesq pour la variation de densité montrent un bon accord avec les mesures faites sur une enceinte avec partition. Excepté aix faibles nombres de Rayleigh, une bulle de séparation est observée derrière le baffle. L'intensité de cette bulle augmente tandis que le mouvement principal s'atténue (ascension à la paroi chaude et descente à la paroi froide) lorsque la conductivité de baffle augmente. Le nombre de Nusselt moyen pour l'enceinte est significativement plus faible en présence des baffles. Excepté aux faibles nombres de Rayleigh (lorsque la conductivité de baffle a une faible influence), les valeurs du nombre de Nusselt diminuent quand la conductivité de baffle croît.

WÄRMEÜBERGANG BEI FREIER KONVEKTION IN EINEM TEILWEISE UNTERTEILTEN SENKRECHTEN HOHLRAUM MIT LEITENDER DECK- UND BODENWAND

Zusammenfassung—Eine numerische Untersuchung der natürlichen Konvektion in einem Hohlraum mit unendlich gut leitender horizontaler Deck- und Bodenwand und Leitblechen mit endlicher Wärmeleitfähigkeit wurde durchgeführt. Die mit Hilfe der Boussinesq-Approximation für die Dichteänderung ermittelten Ergebnisse zeigen eine gute Übereinstimmung mit Messungen der natürlichen Konvektion in unterteilten Hohlräumen, wie sie in der Literatur zu finden sind. Hinter den Leitblechen wird eine Ablöseblase beobachtet (außer bei kleinen Rayleigh-Zahlen). Die Stärke dieser Ablöseblase nimmt mit der Wärmeleitfähigkeit der Leitbleche zu, während die Stärke der Hauptströmung (aufwärts an der heißen, abwärts an der kalten Wand) abnimmt. Die mittlere Nusselt-Zahl im Hohlraum mit Leitblechen ist viel kleiner als ohne Leitbleche. Die Nusselt-Zahl nimmt mit zunehmender Wärmeleitfähigkeit der Leitbleche ab—außer bei den kleinen Rayleigh-Zahlen (wo die Leitfähigkeit einen geringen Einfluß hat).

СВОБОДНОКОНВЕКТИВНЫЙ ПЕРЕНОС ТЕПЛА В ЧАСТИЧНО ПЕРЕГОРОЖЕННОЙ ВЕРТИКАЛЬНОЙ ПОЛОСТИ С ПРОВОДЯЩИМИ ТОРЦЕВЫМИ СТЕНКАМИ

Аннотация—Проведено численное исследование естественной конвекции в полости с идеально проводящими горизонтальными торцевыми стенками и с перегородками, имеющими конечную теплопроводность. Данные, полученные с использованием модели Буссинеска для описания изменения плотности, хорошо согласуются с опубликованными результатами измерений естественной конвекции в полости, разделенной перегородками. За исключением случаев малых чисел Рэлея за перегородкой наблюдается вихревое течение. Интенсивность этого течения увеличивается, в то время как интенсивность основного потока (движущегося по нагретой стенке вверх и по холодной стенке вниз) уменьшается с увеличением теплопроводности перегородки. Среднее значение числа Нуссельта для полости значительно ниже при наличии перегородок. За исключением случаев малых чисел Рэлея (когда теплопроводность перегородки оказывает небольшое влияние), числа Нуссельта уменьшаются с ростом теплопроводности перегородок.